Electronic Supplementary Information for:

Thermodynamic Stability, Phase Separation and Ag Grading in $(Ag,Cu)(In,Ga)Se_2$ Solar Absorbers

Kostiantyn V. Sopiha[1], Jes K. Larsen[1], Olivier Donzel-Gargand[1], Faraz Khavari[1], Jan Keller[1], Marika Edoff[1], Charlotte Platzer-Björkman[1], Clas Persson[2,3], and Jonathan J. S. Scragg[1]

[1]Solar Cell Technology, Department of Materials Science and Engineering, Uppsala University, Box 534, SE-75121 Uppsala, Sweden

[2]Department of Materials Science and Engineering, KTH Royal Institute of Technology, SE-100 44 Stockholm, Sweden

[3]Center for Materials Science and Nanotechnology/Department of Physics, University of Oslo, P.O. Box 1048 Blindern, NO-0316 Oslo, Norway

Table S1. Computed formation enthalpies and lattice parameters of ternary chalcopyrite systems. The calculations were performed on the primitive cells using *Γ*-centred Monkhorst-Pack grids with density of 3000 k-points per reciprocal atom and cut-off energy of 550 eV.

Compound	Formation enthalpy (eV/formula)	Lattice constants (Å)	
		a	c
$CuGaSe_2$	-1.9287	5.6798	11.2680
$CuInSe_2$	-1.7819	5.8797	11.8160
$AgGaSe_2$	-1.8244	6.0604	11.2622
$AgInSe_2$	-1.7213	6.2055	12.0825

Table S2. Parameters of the investigated ACIGS films: sample names, compositions as measured by XRF, types of substrates, co-evaporation stages at which Ag was introduced, band gaps, and solar cell characteristics (for best cells). The parameters are obtained for as-grown (non-annealed) films and devices. "N/A" denotes films that were not processed into the devices.

Sample name	XRF composition			Glass type	Ag in stage	E_g (eV)	V_{OC} (mV)	J_{SC} (mA/cm^2)	*FF* (%)	η (%)
	Ag/I	I/III	Ga/III							
AAC05@SLG	0.06	0.88	0.40	SLG	I	1.25	765	29.78	78.83	17.97
AAC10@SLG	0.11	0.80	0.40	SLG	I	1.24	739	30.19	77.75	17.36
AAC20@SLG	0.18	0.79	0.41	SLG	I	1.25	770	28.99	79.01	17.63
AAC05@KRG	0.05	0.87	0.44	KRG	I	1.26	778	30.49	77.51	18.38
AAC10@KRG	0.09	0.80	0.43	KRG	I	1.23	734	31.06	74.42	16.96
AAC20@KRG	0.15	0.76	0.44	KRG	I	1.24	754	31.07	72.78	17.05
AAC05_st1@KRG	0.04	0.91	0.42	KRG	I	N/A				
AAC10_st2@KRG	0.12	0.84	0.44	KRG	II					
AAC05_st3@KRG	0.06	0.91	0.42	KRG	III					
AAC50@SLG	0.51	0.82	0.85	SLG	All	1.57	929	18.30	62.22	10.58

To fabricate the solar cells characterised in Table S2, on top of absorber films, 50 nm CdS buffer was deposited using chemical bath deposition (CBD) for all but AAC50@SLG sample, which instead was covered with 20 nm Zn-Sn-O buffer *via* atomic layer deposition (ALD) at T = 120°C. More details on the buffer deposition can be found in references 5 and 8. The cells were finalized by sputtering i-ZnO(70 nm)/ZnO:Al(210 nm) bi-layer. The devices were characterised by external quantum efficiency (EQE) and current-voltage (IV) measurements at room temperature in home-built setups with an ELH lamp. The band gaps (E_g) were extracted by taking energy at the maximum derivative of EQE.

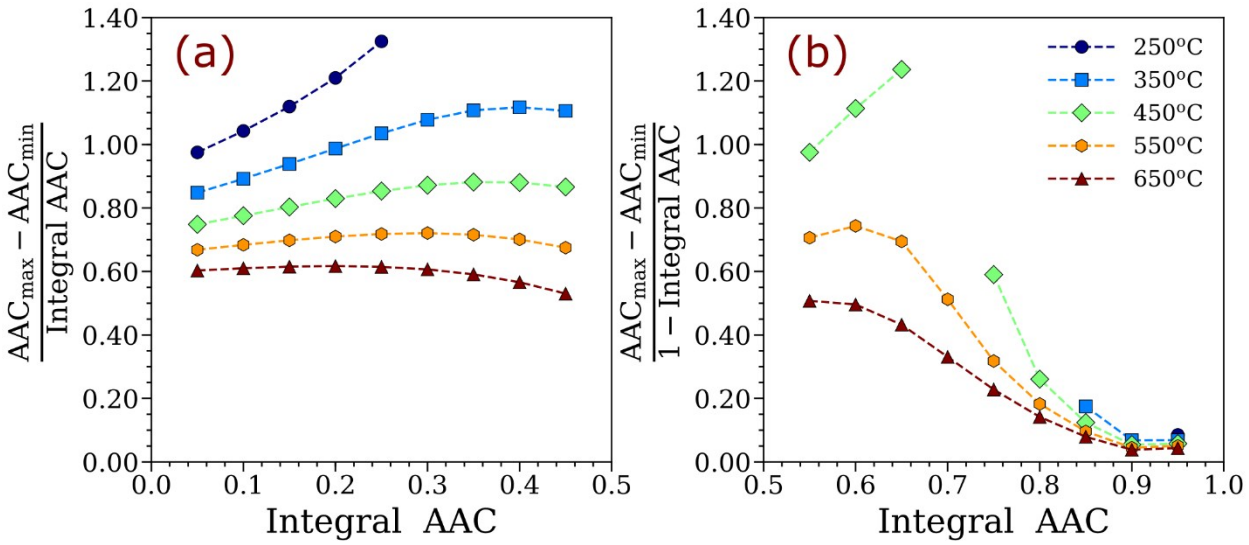

Figure S1. Calculated difference between the maximum and minimum of the optimized AAC profiles (as shown in Figure 3b) divided by (a) integral AAC (if AAC < 0.50) and (b) 1 - integral AAC (if AAC > 0.50) *versus* integral AAC at different temperatures.

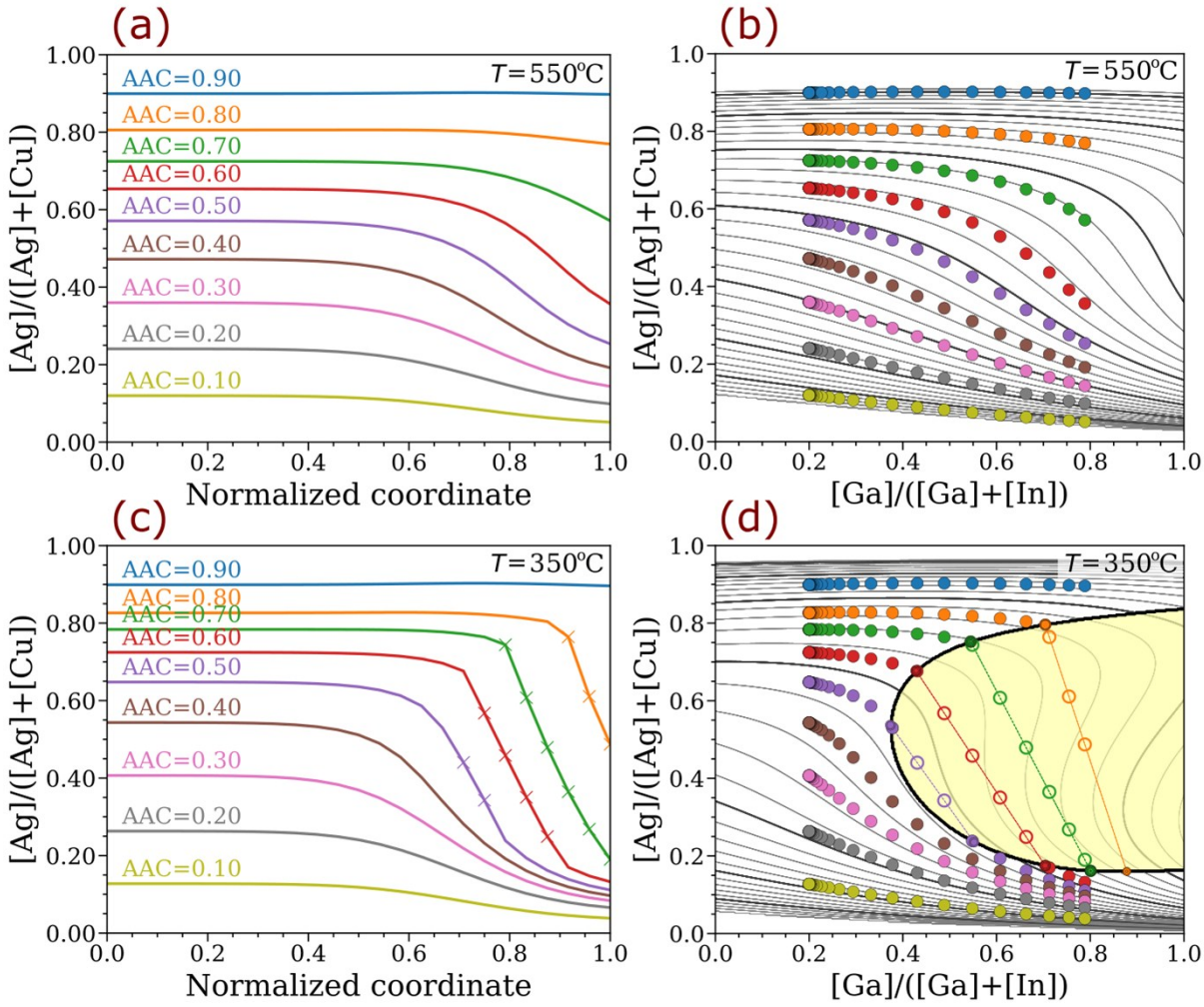

Figure S2. (a,c) Calculated equilibrium model AAC profiles and (b,d) the corresponding compositions of phases formed in each cell of the profiles at (a,b) 550 °C and (c,d) 350 °C. The grey contours in background of (b,d) represent iso-$\partial \Delta G(x,y)/\partial y$ curves. The respective model GGI profile is shown in Figure 3a. (a) is fully equivalent to Figure 3c. The local phase decomposition is indicated in (c) by the cross markers for all cells containing a mixture of two phases; this effect leads to more abrupt AAC profiles. The overall compositions of the phase mixtures for each decomposed cell are shown by the open markers in (d). Compositions of the stable phases are shown by solid markers joined by the dashed lines, where the phase amounts are proportional to the marker sizes. As one can see, at 350 °C, the local decomposition occurs when any region of the profile (for $0.50 \leq \text{AAC} \leq 0.80$) enters under the binodal line, and thus, such an alloy splits into two phases with compositions at the binodal line. All profiles with local phase decomposition are excluded from evaluating the extent of AAC grading (see Figure 3d) because phase segregation and AAC profiling may occur at different times scales.

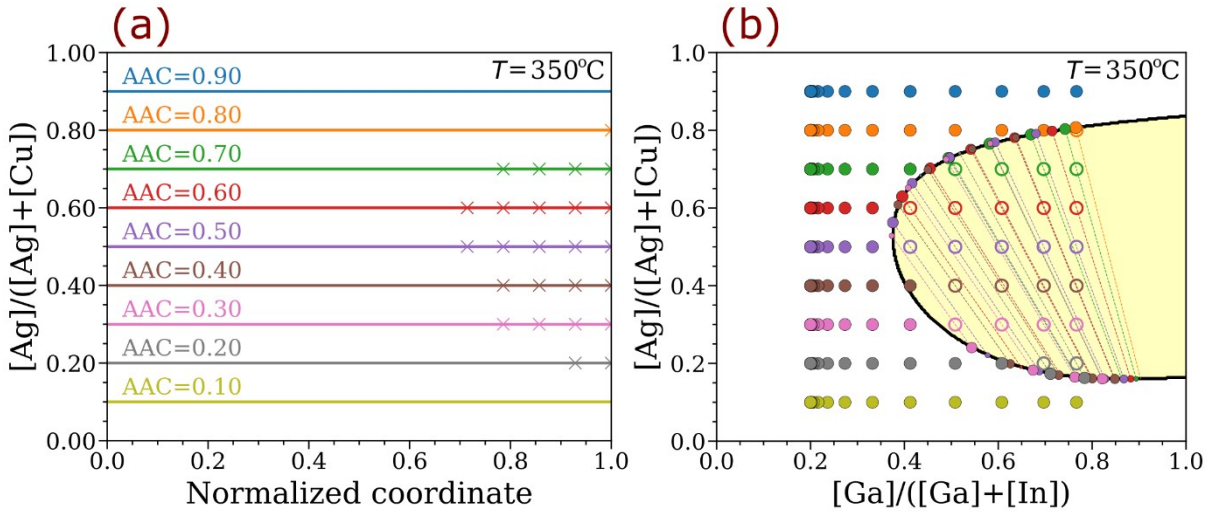

Figure S3. Same parameters as in Figure S2c,d but computed for a fixed AAC profile (allowing the phase separation within each cell only); this situation represents a hypothetical case when kinetics of the phase decomposition is much faster than that of AAC profiling. Here, the number of cells is decreased to 15 for clarity. In contrast to Figure S2c,d, the decomposition ***always*** occurs in Ga-rich region near the back contact and at significantly lower integral AAC.

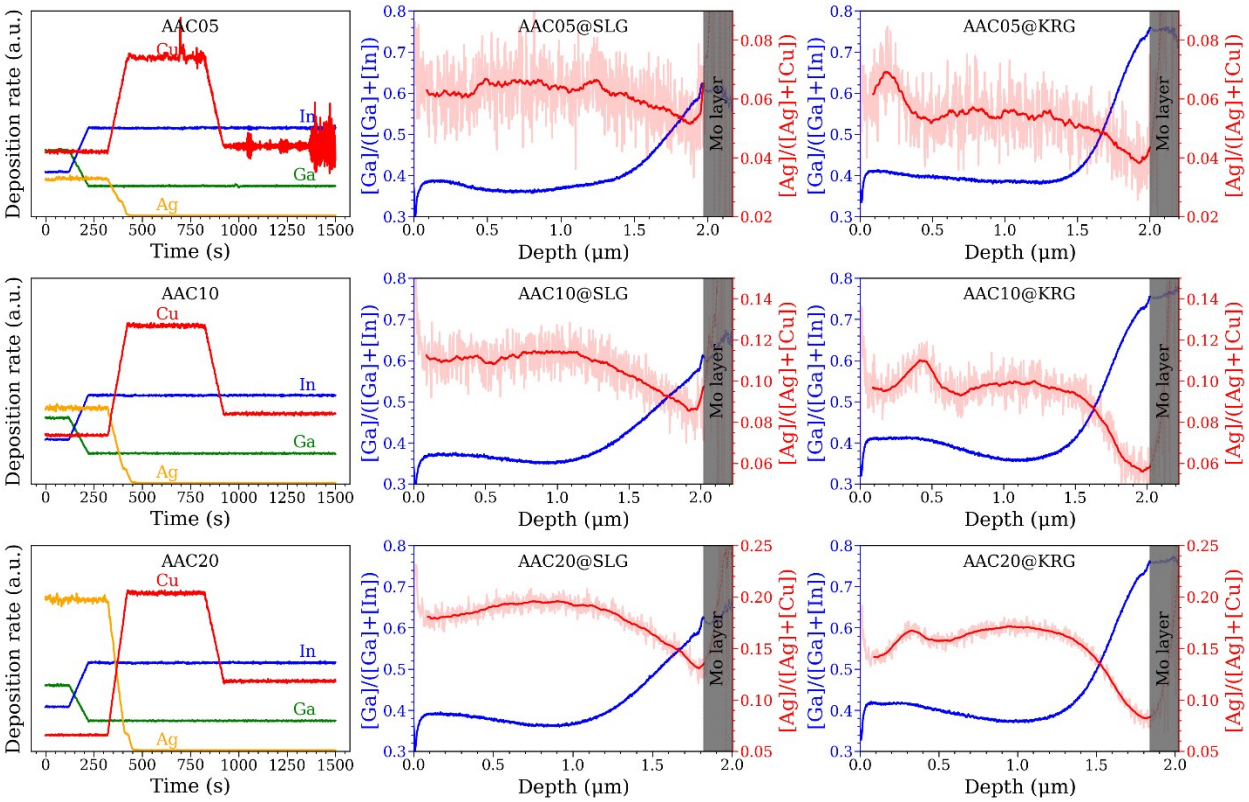

Figure S4. AAC and GGI distributions in ACIGS films with different Ag content. Estimated concentration protocols for cations during co-evaporation (left column); GDOES profiles measured for the absorbers deposited on soda-lime glass (middle column) and K-rich/Na-poor glass (right column). The anticorrelation between GGI and AAC is evident in all samples irrespective of the substrate type. The near-surface perturbations are OVC grains formed in the absorbers deposited on K-rich/Na-poor glass (see Figure 4b).

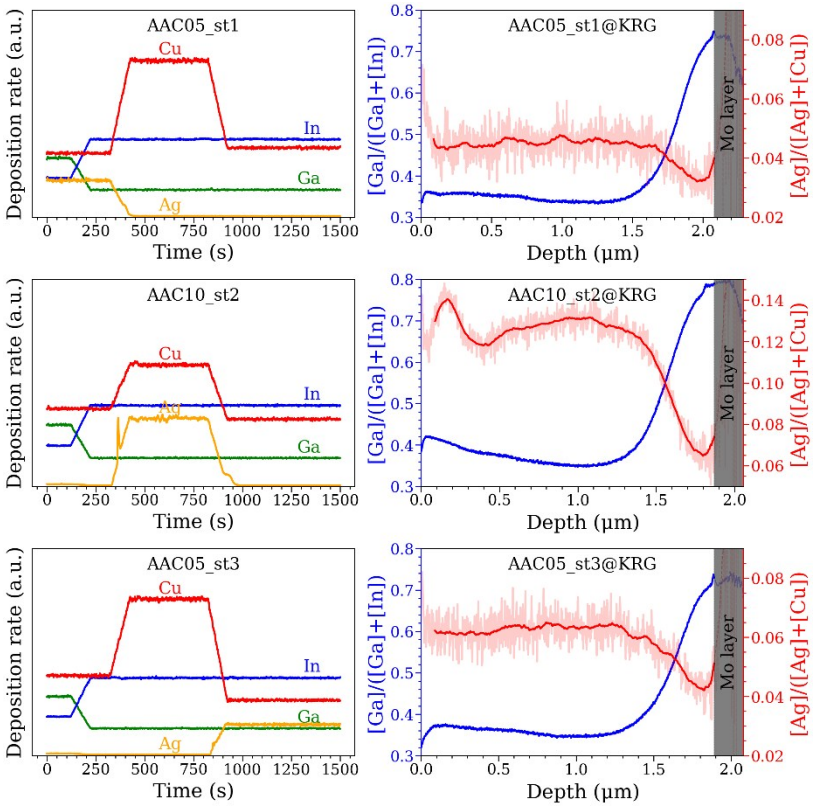

Figure S5. AAC and GGI distribution in ACIGS with Ag incorporated at different deposition stages. Estimated concentration protocols for cations during the co-evaporation (left column) and measured GDOES profiles (right column). The AAC profiles are qualitatively similar irrespective of when Ag was introduced, with a clear anticorrelation between GGI and AAC. The near-surface perturbations are OVC grains formed in the absorbers deposited on K-rich/Na-poor glass (see Figure 4b).

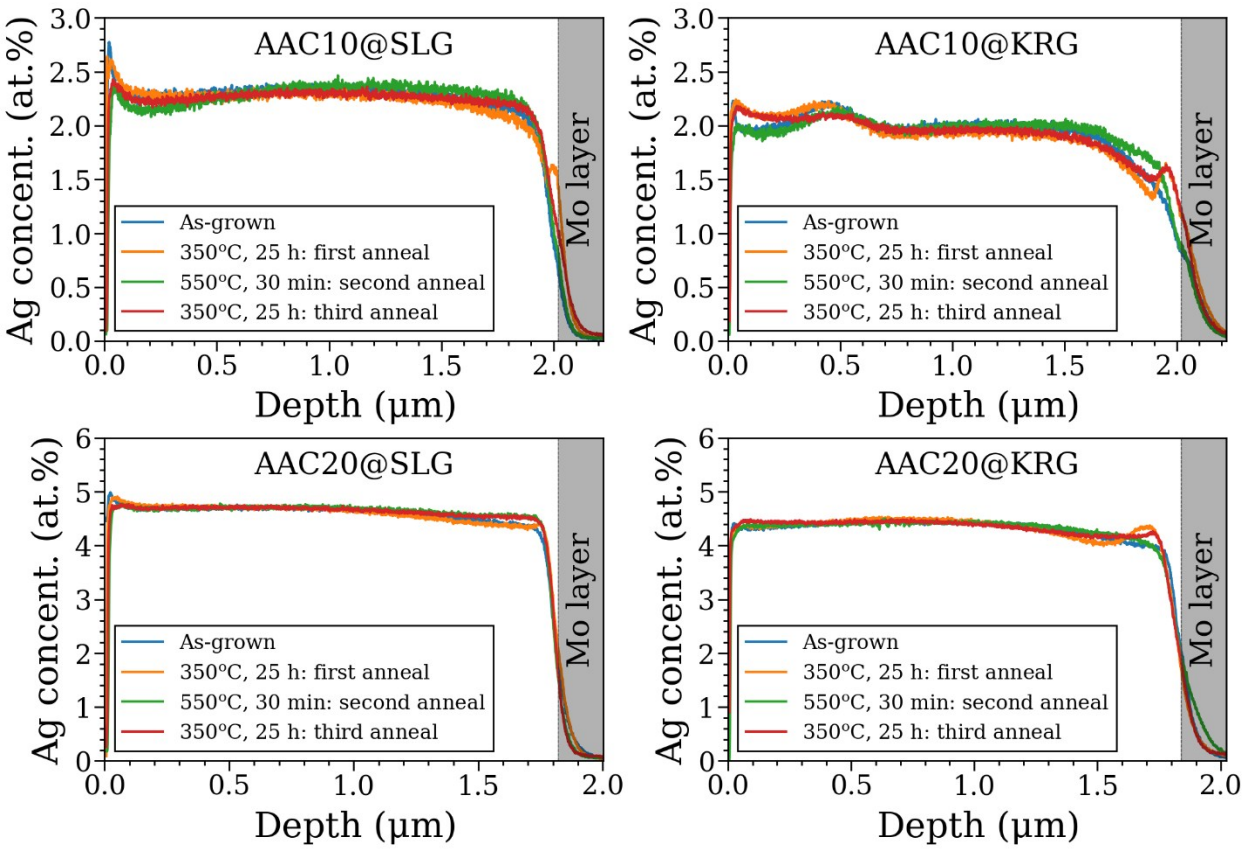

Figure S6. Ag profiles in ACIGS film before and after sequential post-deposition heat treatments, as measured by GDOES.

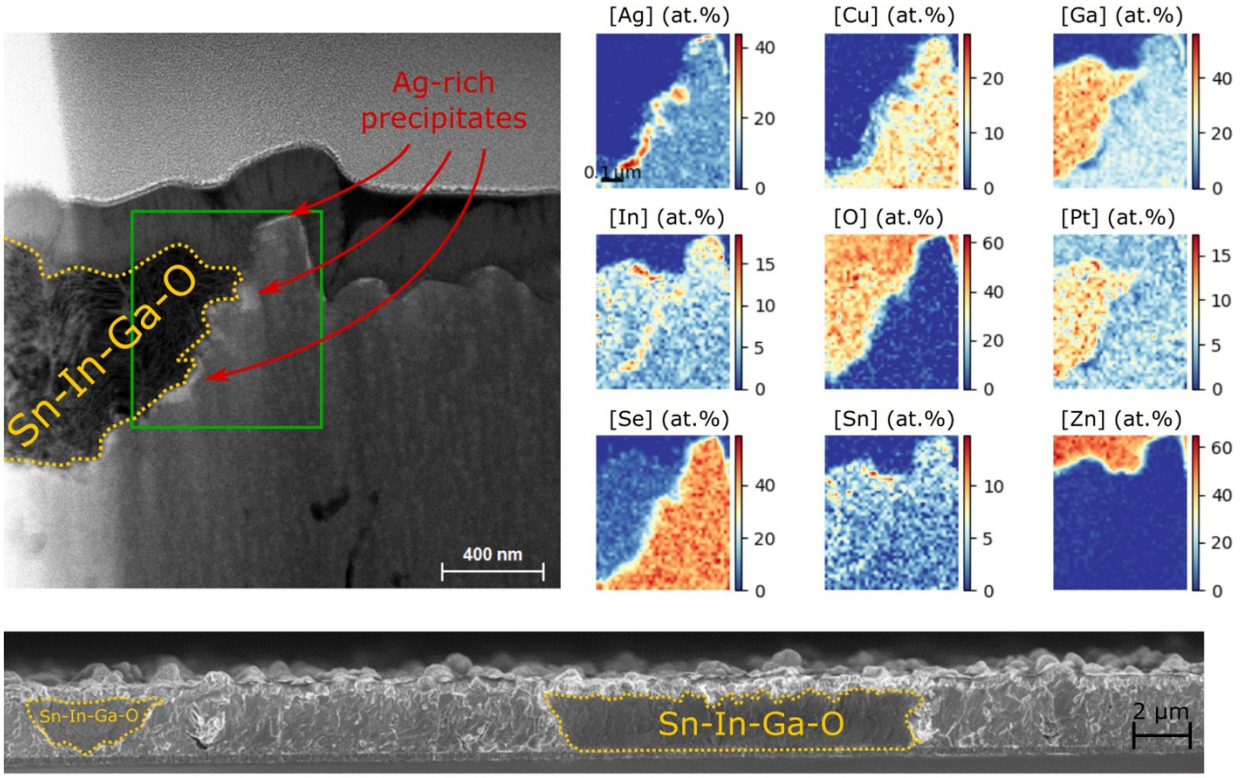

Figure S7. Cross-section STEM-EDS (top) and SEM (bottom) analyses of ACIGS film with AAC = 0.50 and GGI = 0.85 (AAC50@SLG sample in Table S2) after heat treatment at 350ºC for 60 hours. An extensive degradation *via* formation of Sn-In-Ga-O regions is revealed by both imaging techniques. The effect is a consequence of Zn-Sn-O (ZTO) buffer layer being present during the annealing. It is unclear whether this degradation is fundamentally driven by the same thermodynamic force as precipitation of Ag-rich grains, which are also seen at the interface between ACIGS and Sn-In-Ga-O patches.